

Constraints on non-linear tides due to p - g mode coupling from the neutron-star merger GW170817

STEVEN REYES¹ AND DUNCAN A. BROWN¹

¹*Syracuse University, Syracuse, NY 13244, USA*

Submitted to ApJ

ABSTRACT

It has been suggested by [Weinberg et al. \(2013\)](#) that an instability due to nonlinear coupling of a neutron star's tide to its p - and g -modes could affect the gravitational-wave phase evolution of a neutron-star binary. [Weinberg \(2016\)](#) suggests that this instability can turn on as the gravitational-waves pass through the sensitive band of ground-based detectors, although the size of the effect is not known. The discovery of the binary neutron star merger GW170817 provides an opportunity to look for evidence of nonlinear tides from p - g mode coupling. We compute Bayesian evidences that compare waveform models that include the p - g mode coupling to models that do not. We find that the observations of GW170817 strongly disfavor the existence of p - g mode coupling with Bayes factors $\log_{10} \mathcal{B} < -4$. We conclude that the observation of GW170817 does not support the existence of nonlinear tides due to p - g mode coupling in binary neutron stars.

Keywords: binaries: close - stars: neutron - stars: oscillations

1. INTRODUCTION

The discovery of the binary neutron star merger GW170817 ([Abbott et al. 2017](#)) has given us a new way to explore the physics of neutron stars. Recent studies have measured the star's tidal deformability and placed constraints on the equation of state of the neutron stars ([Abbott et al. 2017](#); [Tews et al. 2018](#); [Most et al. 2018](#); [Raithel et al. 2018](#); [De et al. 2018](#); [Abbott et al. 2018a,b](#)). [Weinberg et al. \(2013\)](#) have suggested that the star's tidal deformation can induce non-resonant and non-linear daughter wave excitations in p - and g -modes of the neutron stars via a quasi-static instability. This instability would remove energy from a binary system and possibly affect the phase evolution of the gravitational waves radiated during the inspiral. Although [Venumadhav et al. \(2014\)](#) concluded that there is no quasi-static instability and hence no effect on the inspiral, [Weinberg \(2016\)](#) claims that the instability can rapidly drive modes to significant energies well before the binary merges. However, the details of the instability saturation are unknown and so the size of the effect of the p - g mode coupling on the gravitational-waveform is not known ([Weinberg 2016](#)). The discovery of the binary neutron star merger GW170817 by Advanced LIGO and Virgo provides an opportunity to determine if there is evidence for non-linear tides from p - g mode coupling during the binary inspiral.

In this paper, we use Bayesian inference to place constraints on non-linear tides during the inspiral of GW170817. Since the physics of the p - g mode instability is uncertain, [Essick et al. \(2016\)](#) developed a parameterized model of the energy loss due to non-linear tides. This model is parameterized by the amplitude and the frequency dependence of the energy loss, and the gravitational-wave frequency at which the instability saturates and the energy loss turns on. For plausible assumptions about the saturation, [Essick et al. \(2016\)](#) concluded that $> 70\%$ of binary merger signals could be missed if only point-particle waveforms are used, and that non-linear tides may significantly bias the measured parameters of the binary. We use Bayesian model selection to compare two models of the gravitational waves radiated during the inspiral of GW170817. The first model is that used by [De et al. \(2018\)](#) to measure the tidal deformability and radii of the neutron stars. Using the parameterized energy loss due to non-linear tides given

by [Essick et al. \(2016\)](#), we construct a second model that includes the leading-order effect of the p - g mode coupling on the wave’s phasing. The PyCBC Inference package ([Nitz et al. 2018](#); [Biwer et al. 2018](#)) is used to calculate Bayes factors comparing these models, hence determining which hypothesis is supported by the observations.

We find that the gravitational-wave observations of GW170817 strongly favor the model that does not include the additional energy loss due to non-linear tides, with Bayes factors $\log_{10} \mathcal{B} < -4$ for all the prior distributions that we explored. By investigating marginalized posterior probability for the binary’s parameters, we find that a non-trivial amount of gravitational-wave phase shift from the non-linear tides happens when either the effect enters the waveform in a way that is degenerate with the binary’s chirp mass ([Peters & Mathews 1963](#)), or turns on at frequencies higher than the most sensitive band of the gravitational-wave detectors. Since the Bayes factors strongly favor the simpler model that does not include non-linear tides, we conclude that the observations of GW170817 do not support evidence for non-linear tides due to p - g mode coupling.

2. WAVEFORM MODEL

As two neutron stars orbit each other, they lose orbital energy E_{orbital} due to gravitational radiation \dot{E}_{GW} . The gravitational waveform during the inspiral is well modeled by post-Newtonian theory (see e.g. [Blanchet \(2014\)](#)). The effect of the p - g mode instability is to dissipate orbital energy by removing energy from the tidal bulge of the stars ([Weinberg et al. 2013](#); [Weinberg 2016](#); [Essick et al. 2016](#)). Once unstable, the coupled p - and g -modes are continuously driven by the tides, giving rise to an extra energy dissipation \dot{E}_{NL} for each star in the standard energy-balance equation ([Peters & Mathews 1963](#))

$$\dot{E}_{\text{orbital}} = -\dot{E}_{\text{GW}} - \dot{E}_{\text{NL}}^1 - \dot{E}_{\text{NL}}^2. \quad (1)$$

Since the details of how the nonlinear tides extract energy from the orbit is not known, [Essick et al. \(2016\)](#) constructed a simple model of the energy loss and calculated plausible values for the model’s parameters. In this model, the rate of orbital energy lost during the inspiral is modified by

$$\dot{E}_{\text{NL}} \propto A f^{n+2} \Theta(f - f_0), \quad (2)$$

where A is a dimensionless constant that determines the overall amplitude of the energy loss, n determines the frequency dependence of the energy loss, and f_0 is the frequency at which the p - g mode instability saturation occurs and the effect turns on. By solving Eq. (1), [Essick et al. \(2016\)](#) computed the leading-order effect of the nonlinear tides on the gravitational-wave phase as a function of A , n , and f_0 . In this analysis, they allowed each star to have independent values of A , f_0 , and n , but found that the energy loss due to nonlinear tides depends relatively weakly on the binary’s mass ratio. Hence, they consider a model that performs a Taylor expansion in the binary’s component mass ([Del Pozzo et al. 2013](#)) and include only the leading-order terms in the binary’s phase evolution. Given this, we parameterize our nonlinear tide waveform with a single set of parameters A , n , and f_0 , by setting $\dot{E}_{\text{NL}}^1 = \dot{E}_{\text{NL}}^2$ and keeping only the leading-order terms nonlinear tide terms when we obtain the quantities $t(f)$ and $\phi(f)$ used to compute the stationary phase approximation ([Sathyaprakash & Dhurandhar 1991](#); [Droz et al. 1999](#); [Lindblom et al. 2008](#)). This approach is reasonable for GW170817, since both neutron stars have similar masses and radii ([De et al. 2018](#)).

The dependence of A , n , and f_0 on the star’s physical parameters is not known ([Weinberg 2016](#)). [Essick et al. \(2016\)](#) estimate that plausible parameter ranges are $A \lesssim 10^{-6}$, $0 \lesssim n \lesssim 2$, and $30 \lesssim f_0 \lesssim 80$ Hz. [Zhou & Zhang \(2018\)](#) found that the frequency at which the instability begins to grow is equation-of-state dependent and can occur at gravitational-wave frequencies as high as 700 Hz. [Andersson & Ho \(2018\)](#) suggest that the instability may only act during the late stages of inspiral, (above 300 Hz), otherwise the large energy dissipation will cause the temperature of the neutron stars to be very large.

In this paper, we compare two models for the gravitational waves radiated by GW170817. The first is the standard restricted stationary-phase approximation to the Fourier transform of the gravitational waveform $\tilde{h}(f)$, known as the TaylorF2 waveform ([Sathyaprakash & Dhurandhar 1991](#)). We begin with the same waveform model used by [De et al. \(2018\)](#), which is accurate to 3.5 PN order in the orbital phase, 2.0 PN order in spin-spin, self-spin and quadrupole-monopole interactions, 3.5 PN order in spin-orbit coupling, and includes the leading and next-to-leading order corrections from the star’s tidal deformability ([Kidder et al. 1993](#); [Blanchet et al. 1995, 2004](#); [Buonanno et al. 2009](#); [Arun et al. 2009](#); [Marsat et al. 2014](#); [Boh et al. 2013, 2015](#); [Mikoczi et al. 2005](#); [Flanagan & Hinderer 2008](#); [Vines et al. 2011](#)). We then construct a second model that adds the leading order effect of nonlinear tides computed using

the model of [Essick et al. \(2016\)](#). We compute the Fourier phase for the TaylorF2 model $\Psi(f)_{\text{TaylorF2}}$ and add a term that accounts for the additional energy lost nonlinear tides $\Psi_{\text{NL}}(f)$, given by

$$\Psi_{\text{NL}}(f) = -\frac{25}{768}A \left(\frac{G\mathcal{M}\pi f_{\text{ref}}}{c^3} \right)^{-\frac{10}{3}} \times \begin{cases} \left(\frac{f_0}{f_{\text{ref}}} \right)^{n-3} \left[\left(\frac{f}{f_0} \frac{1}{n-4} \right) - \frac{1}{n-3} \right] & f < f_0, \\ \left(\frac{f}{f_{\text{ref}}} \right)^{n-3} \left(\frac{1}{n-4} - \frac{1}{n-3} \right) & f \geq f_0. \end{cases} \quad (3)$$

Here, f_{ref} is a reference frequency which we set to 100 Hz following [Essick et al. \(2016\)](#), G is Newton’s gravitational constant, c is the speed of light, and $\mathcal{M} = (m_1 m_2)^{3/5} / (m_1 + m_2)^{1/5}$ is the chirp mass of the binary.¹ We generate the standard TaylorF2 waveform using the LIGO Algorithm Library ([Mercer et al. 2017](#)) and multiply this frequency-domain waveform by the term due to the nonlinear tides,

$$\tilde{h}_{\text{TaylorF2+NL}}(f) = \tilde{h}_{\text{TaylorF2}}(f) \times \exp[-i\Psi_{\text{NL}}(f)]. \quad (4)$$

The Fourier phase for the non-linear tides is implemented as a patch to the version of the PyCBC software ([Nitz et al. 2018](#)) used by [De et al. \(2018\)](#). Both the standard and nonlinear tide waveform models are terminated when the gravitational-wave frequency reaches that of a test particle at the innermost stable circular orbit of a Schwarzschild black hole of mass $M = m_1 + m_2$. For the neutron star masses considered here, this frequency is between 1.4 kHz and 1.6 kHz.

3. METHODS

We use Bayesian model selection to determine which of the two waveform models described in [Sec. 2](#) is better supported by the observations of GW170817. Bayes’ theorem states that

$$p(H, \vec{\theta} | \mathbf{d}) = \frac{p(\mathbf{d} | H, \vec{\theta}) p(\vec{\theta} | H)}{p(\mathbf{d} | H)}, \quad (5)$$

where $p(\mathbf{d} | H)$ is the evidence (or marginal likelihood) of the model H , $p(\vec{\theta} | H)$ is the prior distribution of the parameters given the signal model, and $p(\mathbf{d} | H, \vec{\theta})$ is the likelihood of the data for a particular set of parameters $\vec{\theta}$. The likelihood used in this analysis assumes a Gaussian model of detector noise and depends upon the noise-weighted inner product between the gravitational waveform and the data from the gravitational-wave detectors ([Finn 2001](#); [Rover et al. 2007](#)). The Bayes factor \mathcal{B} that we use to compare our two models is given by

$$\mathcal{B} = \frac{p(\mathbf{d} | H_{\text{TaylorF2+NL}})}{p(\mathbf{d} | H_{\text{TaylorF2}})}. \quad (6)$$

This is the evidence ratio between hypotheses that include and exclude the effect of nonlinear tides. Posterior distributions for parameters of interest can be also computed by marginalizing the posterior probability distribution over other parameters. Marginalization to obtain the posterior probabilities and the evidence is performed using Markov Chain Monte Carlo (MCMC) techniques. To compute posterior probability distributions and evidences, we use the *PyCBC Inference* software ([Nitz et al. 2018](#); [Biver et al. 2018](#)) using the the parallel-tempered *emcee* sampler ([Foreman-Mackey et al. 2013](#); [Vousden et al. 2016](#)). This sampler allows the use of multiple temperatures to dampen the likelihood function ([Foreman-Mackey et al. 2013](#); [Wang & Swendsen 2005](#); [Earl & Deem 2005](#)). The evidence accumulated from these different temperatures are then incorporated into the evidence calculation according to their modified likelihood functions ([Foreman-Mackey et al. 2013](#); [Biver et al. 2018](#)).

We use the gravitational-wave strain data from the Advanced LIGO and Virgo detectors for the GW170817 event, made available through the LIGO Open Science Center ([Vallisneri et al. 2015](#); [Blackburn et al. 2017](#)). We fix the sky location and distance to GW170817 ([Soares-Santos et al. 2017](#); [Cantiello et al. 2018](#)) and assume that both neutron stars have the same equation of state by imposing the common radius constraint ([De et al. 2018](#)). In the case of the standard TaylorF2 waveform $H = \tilde{h}_{\text{TaylorF2}}$, our analysis is identical to that described in [De et al.](#)

¹ Appendix A of [Essick et al. \(2016\)](#) gives the change to the gravitational-wave phase $\phi(f)$ as a function of frequency and not the change to the Fourier phase $\Psi(f)$ (see e.g. [Lindblom et al. \(2008\)](#) for a discussion of how these differ). The former quantity is useful to compute the change in the number of gravitational-wave cycles, but the latter is required to compute the modification to the TaylorF2 waveform.

(2018). This analysis considered three prior distributions on the binary’s component mass. Here, we only consider uniform priors on each star’s mass, with $m_{1,2} \sim U[1, 2] M_\odot$, and a Gaussian prior on the component masses $m_{1,2} \sim N(\mu = 1.33, \sigma = 0.09) M_\odot$ (Ozel & Freire 2016). For both mass priors, we restrict the chirp mass to the range $1.1876 M_\odot < \mathcal{M} < 1.2076 M_\odot$. Since our analysis is identical to that of De et al. (2018), we refer to that paper for the details of the data analysis configuration. For the denominator of Eq. (6), we use the evidence $p(\mathbf{d}|H_{\text{TaylorF2}})$ provided as supplemental materials by De et al. (2018).

We then repeat the analysis of De et al. (2018) using the waveform model $H = \tilde{h}_{\text{TaylorF2+NL}}$ to compute the evidence $p(\mathbf{d}|H_{\text{TaylorF2+NL}})$. Given the uncertainty on the range of the nonlinear tide parameters, we draw $n \in U[-1.1, 2.999]$, and A from a distribution uniform in \log_{10} between 10^{-10} and 10^{-6} . We investigate two choices of drawing f_0 : we draw f_0 from a uniform distribution between 15 and 100 Hz, as used by Essick et al. (2016), and from a uniform distribution between 15 and 800 Hz to allow for the larger values of f_0 suggested by Zhou & Zhang (2018) and Andersson & Ho (2018). Since some combinations of A , n , and f_0 can produce extremely small gravitational-wave phase shifts (Essick et al. 2016), we place a cut on the gravitational-wave phase shift due to nonlinear tides

$$\delta\phi(f_{\text{ISCO}}) = \frac{-25}{768} \frac{A}{n-3} \left(\frac{GM\pi f_{\text{ref}}}{c^3} \right)^{-10/3} \left(\frac{f_{\text{ISCO}}}{f_{\text{ref}}} \right)^{n-3}, \quad (7)$$

where f_{ISCO} is the termination frequency of the waveform (which is always larger than f_0 in our analysis). We restrict the prior space to values of $\delta\phi \geq 0.1$ rad. For a $m_1 = m_2 = 1.4 M_\odot$ binary, values of (A, f_0, n) that produce phase shifts of $\delta\phi \approx 0.1$ rad have matches between the two waveform models greater than 99.98%. This cut means that the resulting priors on A , n , and f_0 are not uniform, but are biased in favor of combinations of parameters that can produce a measurable effect due to nonlinear tides. The priors on A , n , and f_0 and the resulting prior on $\delta\phi(f_{\text{ISCO}})$ are shown in Fig. 1.

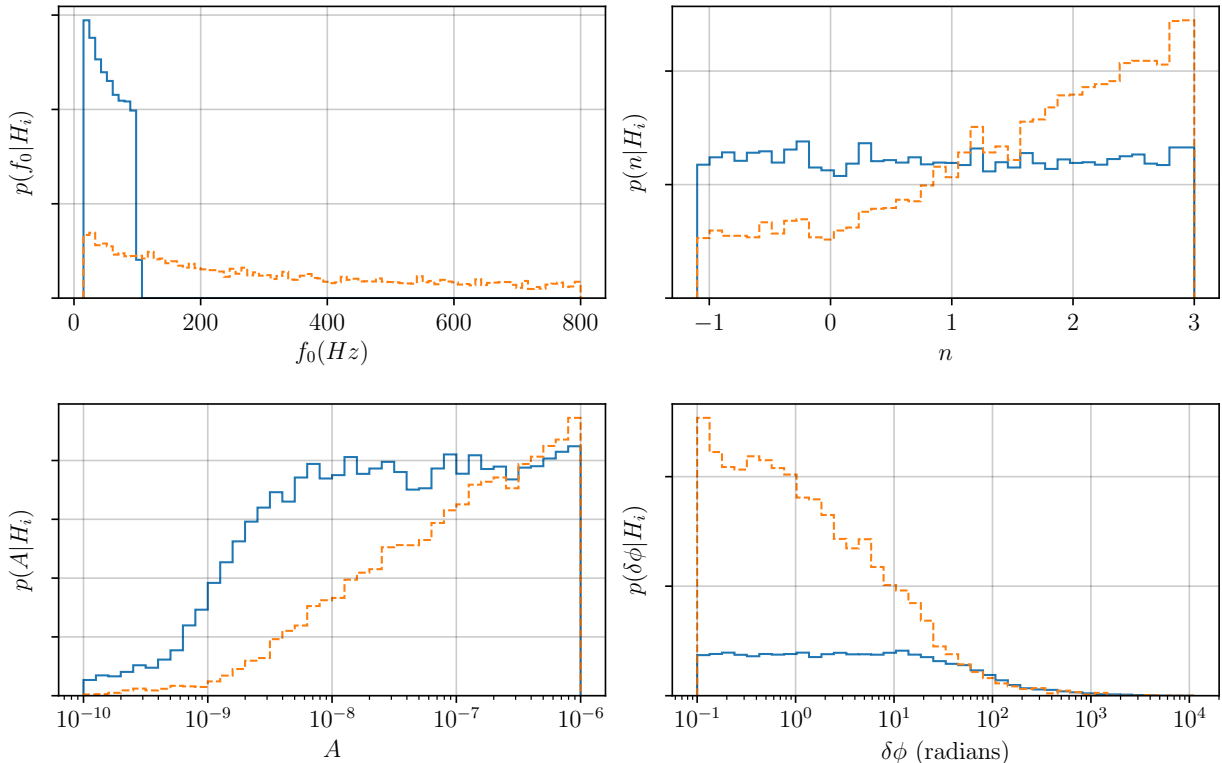


Figure 1. Prior probability distributions on the parameters (f_0, n, A) for the waveform model $H_i = \tilde{h}_{\text{TaylorF2+NL}}(f)$ and the resulting prior on the gravitational-wave phase shift $\delta\phi$ due to nonlinear tides. The cut $\delta\phi \geq 0.1$ rad has been applied when generating these priors. The solid (dashed) lines shows the priors when f_0 is drawn from a uniform distribution between 15 and 100 Hz (800 Hz). The prior on the amplitude is biased towards large amplitudes that give larger phase shifts.

4. RESULTS

We find that in all cases, the Bayes factors for GW170817 strongly favor the simpler model $H = \tilde{h}_{\text{TaylorF2}}(f)$ that does not include the effect of nonlinear tides from p - g mode coupling. This is true independent of the mass prior distribution, or the range of f_0 considered. For the smaller range of $15 \leq f_0 \leq 100$ Hz suggested by [Essick et al. \(2016\)](#), we find that the Bayes factors are $\log_{10} \mathcal{B} = -9.2, -6.0$ for the uniform mass prior and Gaussian mass prior, respectively. For the broader range $15 \leq f_0 \leq 800$ Hz, we find that $\log_{10} \mathcal{B} = -6.3, -4.7$ for the uniform mass prior and Gaussian mass prior, respectively.

One might naïvely expect that if the p - g mode coupling does not affect neutron stars, then the smallest Bayes factor would be obtained when comparing the standard model to the nonlinear tide model with the largest prior probability space, due to its larger Occam factor. When comparing the mass prior spaces for a given range of f_0 , we do see this. However, we see that the smallest Bayes factor is obtained for the uniform mass prior with the smaller prior range of f_0 , $\log_{10} \mathcal{B} = -9.2$, whereas the larger prior range of f_0 has a Bayes factor of $\log_{10} \mathcal{B} = -6.3$. To understand this, we investigated the marginalized posterior probability densities for the parameters of the model $H = \tilde{h}_{\text{TaylorF2+NL}}(f)$. For the uniform mass distribution, these are shown in [Fig 2](#) for $15 \leq f_0 \leq 100$ Hz and in [Fig. 3](#) for $15 \leq f_0 \leq 800$ Hz (the posteriors for Gaussian mass prior are qualitatively very similar).

When we consider the way that the nonlinear tides enter the Fourier phase in [Eq. \(3\)](#), we see that if $n = 4/3$ then the nonlinear tides enter the Fourier phase of the waveform with the same power law dependence on frequency f as the chirp mass, that is $\Psi(f) \propto f^{-5/3}$. We also note that for the effect of nonlinear tides to be degenerate with chirp mass, they must turn on at a frequency f_0 that is close to the low-frequency limit of the detector’s sensitive band. If the effect turns on at higher frequencies, then the phasing will change in the detector’s sensitive band and it is more difficult to compensate for the nonlinear tide effect with a change in chirp mass.

Our results are consistent with this understanding of the phasing. The marginalized posteriors shown in [Fig. 2](#) show a strong degeneracy between the source-frame chirp mass \mathcal{M}^{src} and non-linear tides that causing a second peak in the chirp mass posterior at lower values of chirp mass than the value measured using the standard waveform model, $\mathcal{M}^{\text{src}} = 1.1867 \pm 0.0001 M_{\odot}$ ([De et al. 2018](#)). We see a peaks in the posteriors of n and f_0 at $n \approx 4/3$ and $f_0 \lesssim 25$ Hz. Since there are also degeneracies with the mass ratio and spin the peaks are not exactly at the predicted values, but the chirp mass degeneracy is the leading order effect. The samples with large posterior values of $\delta\phi$ seen at bottom right in [Fig. 3](#) are strongly correlated with source-frame chirp masses $\mathcal{M}^{\text{src}} \lesssim 1.1866$. We have repeated this analysis changing the low-frequency cutoff of the likelihood from 20 Hz to 25 Hz, and to 30 Hz. In these analyses, the peak in the posterior of f_0 tracks the low-frequency cutoff, confirming that this is due to the chirp-mass degeneracy.

The $n \approx 4/3$ chirp mass degeneracy is still present in the analysis with the larger range of f_0 , shown in [Fig. 3](#), however it is not as pronounced in the posterior samples due to the larger prior space being explored. In [Fig. 3](#), we note that there is a large volume of the prior space where the nonlinear tide waveform has high overlap with the standard waveform. This is consistent with expectations, as if the nonlinear tide effect turns on at higher gravitational-wave frequencies, then the LIGO and Virgo detectors will be less sensitive to its effect. Overall we note the larger volume of prior space with high likelihood values in [Fig. 3](#) compared to [Fig. 2](#), which is consistent with the Bayes factors obtained.

5. DISCUSSION

In this paper, we have used the GW170817 signal and the model of [Essick et al. \(2016\)](#) to look for evidence of non-linear tides from p - g mode coupling during the inspiral ([Weinberg et al. 2013](#); [Weinberg 2016](#); [Zhou & Zhang 2018](#)). Our Bayes factors strongly of $\log_{10} \mathcal{B} < -4$ strongly favor the standard model that excludes non-linear tides, leading us to conclude that the observations of GW170817 do not support the existence of nonlinear tides. While it is possible that this effect is still present in GW170817, the nonlinear tides would have to have a sufficiently low amplitude or turn on at sufficiently high frequencies that current detectors are not sensitive to its effect.

In principle, one could improve our analysis by keeping higher order terms in the waveforms, or separately parameterizing the amplitude, turn-on frequency, and frequency evolution for each star. However, considering that the GW170817 observations already strongly disfavor the model that includes nonlinear tides, and that the neutron stars merging in GW170817 have similar masses and radii ([De et al. 2018](#)), we do not expect this to affect the main conclusion of our paper.

Improved knowledge of the interior dynamics of neutron star cores and crusts, and its interaction with neutron star magnetic fields may yield a better parametrized model regarding p - g mode instabilities ([Weinberg 2016](#)). Non-linear

tides are poorly understood and the contribution from other stellar oscillation modes may yet contribute to a more accurate picture of the interior dynamics of neutron stars (Andersson & Ho 2018). Future LIGO-Virgo Collaboration observing runs will likely provide new observations of binary neutron star mergers (Abbott et al. 2016). With the expected improvements in detector sensitivity, it may be possible to find evidence for the p - g mode instability in coalescing binary neutron stars in the future.

We thank Soumi De and Daniel Finstad for helpful discussions. We thank Alex Nitz for writing the initial version of the code for non-linear tides in PyCBC. The authors were supported by the National Science Foundation grant PHY-1707954. Computational work was supported by Syracuse University and National Science Foundation grant OAC-1541396. This research has made use of data obtained from the LIGO Open Science Center (<http://www.losc.org>).

Software: PyCBC Inference (Nitz et al. 2018; Biwer et al. 2018), emcee (Foreman-Mackey et al. 2013; Vousden et al. 2016), LIGO Algorithm Library (Mercer et al. 2017), Matplotlib (Hunter 2007), Scipy (Jones et al. 2001–)

REFERENCES

- Abbott, B., et al. 2017, Phys. Rev. Lett., 119, 161101
- Abbott, B. P., et al. 2016, Astrophys. J., 832, L21
- . 2018a, arXiv:1805.11581
- . 2018b, arXiv:1805.11579
- Andersson, N., & Ho, W. C. G. 2018, Phys. Rev., D97, 023016
- Arun, K. G., Buonanno, A., Faye, G., & Ochsner, E. 2009, Phys. Rev., D79, 104023, [Erratum: Phys. Rev.D84,049901(2011)]
- Biwer, C. M., Capano, C. D., De, S., et al. 2018, arXiv:1807.10312
- Blackburn, K., et al. 2017, LOSC CLN Data Products for GW170817, doi:doi:10.7935/K5B8566F. <https://dcc.ligo.org/P1700349/public>
- Blanchet, L. 2014, Living Rev. Rel., 17, 2
- Blanchet, L., Damour, T., Esposito-Farese, G., & Iyer, B. R. 2004, Phys. Rev. Lett., 93, 091101
- Blanchet, L., Damour, T., Iyer, B. R., Will, C. M., & Wiseman, A. 1995, Phys. Rev. Lett., 74, 3515
- Boh, A., Faye, G., Marsat, S., & Porter, E. K. 2015, Class. Quant. Grav., 32, 195010
- Boh, A., Marsat, S., & Blanchet, L. 2013, Class. Quant. Grav., 30, 135009
- Buonanno, A., Iyer, B., Ochsner, E., Pan, Y., & Sathyaprakash, B. S. 2009, Phys. Rev., D80, 084043
- Cantiello, M., et al. 2018, Astrophys. J., 854, L31
- De, S., Finstad, D., Lattimer, J. M., et al. 2018, arXiv:1804.08583
- Del Pozzo, W., Li, T. G. F., Agathos, M., Van Den Broeck, C., & Vitale, S. 2013, Phys. Rev. Lett., 111, 071101
- Droz, S., Knapp, D. J., Poisson, E., & Owen, B. J. 1999, Phys. Rev., D59, 124016
- Earl, D. J., & Deem, M. W. 2005, Phys. Chem. Chem. Phys., 7, 3910.
- Essick, R., Vitale, S., & Weinberg, N. N. 2016, Phys. Rev., D94, 103012
- Finn, L. S. 2001, Phys. Rev., D63, 102001
- Flanagan, E. E., & Hinderer, T. 2008, Phys. Rev., D77, 021502
- Foreman-Mackey, D., Hogg, D. W., Lang, D., & Goodman, J. 2013, Publ. Astron. Soc. Pac., 125, 306
- Hunter, J. D. 2007, Computing In Science & Engineering, 9, 90
- Jones, E., Oliphant, T., Peterson, P., et al. 2001–, SciPy: Open source scientific tools for Python, , , [Online; accessed `today`]. <http://www.scipy.org/>
- Kidder, L. E., Will, C. M., & Wiseman, A. G. 1993, Phys. Rev., D47, R4183
- Lindblom, L., Owen, B. J., & Brown, D. A. 2008, Phys. Rev., D78, 124020
- Marsat, S., Boh, A., Blanchet, L., & Buonanno, A. 2014, Class. Quant. Grav., 31, 025023
- Mercer, R. A., et al. 2017, LIGO Algorithm Library, Commit hash version 8cbd1b7187ce3ed9a825d6ed11cc432f3cfde9a5, <https://git.ligo.org/lscsoft/lalsuite>
- Mikoczi, B., Vasuth, M., & Gergely, L. A. 2005, Phys. Rev., D71, 124043
- Most, E. R., Papenfort, L. J., Dexheimer, V., et al. 2018, arXiv:1807.03684
- Nitz, A., Harry, I., Brown, D., et al. 2018, ligo-cbc/pycbc: Post-O2 Release 8, , , doi:10.5281/zenodo.1208115. <https://doi.org/10.5281/zenodo.1208115>
- Ozel, F., & Freire, P. 2016, Ann. Rev. Astron. Astrophys., 54, 401
- Peters, P. C., & Mathews, J. 1963, Phys. Rev., 131, 435
- Raithel, C., zel, F., & Psaltis, D. 2018, Astrophys. J., 857, L23

- Rover, C., Meyer, R., & Christensen, N. 2007, *Phys. Rev.*, D75, 062004
- Sathyaprakash, B. S., & Dhurandhar, S. V. 1991, *Phys. Rev.*, D44, 3819
- Soares-Santos, M., et al. 2017, *Astrophys. J.*, 848, L16
- Tews, I., Margueron, J., & Reddy, S. 2018, arXiv:1804.02783
- Vallisneri, M., Kanner, J., Williams, R., Weinstein, A., & Stephens, B. 2015, *J. Phys. Conf. Ser.*, 610, 012021
- Venumadhav, T., Zimmerman, A., & Hirata, C. M. 2014, *Astrophys. J.*, 781, 23
- Vines, J., Flanagan, E. E., & Hinderer, T. 2011, *Phys. Rev.*, D83, 084051
- Vousden, W. D., Farr, W. M., & Mandel, I. 2016, *Monthly Notices of the Royal Astronomical Society*, 455, 1919.
- Wang, J.-S., & Swendsen, R. H. 2005, *Progress of Theoretical Physics Supplement*, 157, 317.
- Weinberg, N. N. 2016, *Astrophys. J.*, 819, 109
- Weinberg, N. N., Arras, P., & Burkart, J. 2013, *Astrophys. J.*, 769, 121
- Zhou, Y., & Zhang, F. 2018, arXiv:1801.09675, [*Astrophys. J.*849,114(2017)]

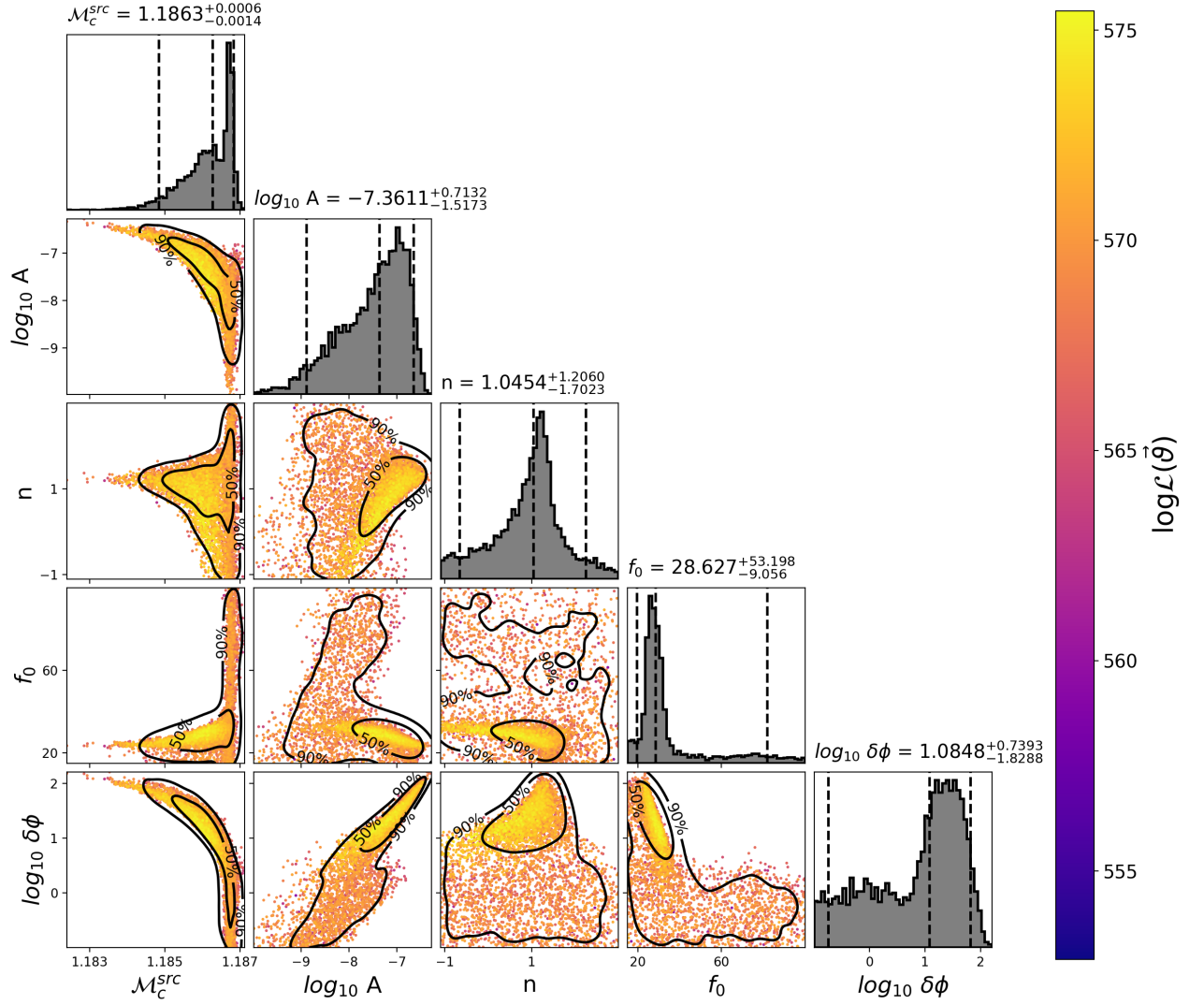


Figure 2. The marginalized posterior distributions for the uniform mass prior and a f_0 restricted to the range 15 and 100 Hz. The vertical lines on the marginalized histograms display the 5th, 50th, and 95th percentiles of the posteriors. The three-detector network log likelihood ratio for each sample is given on the color-bar. The posterior scatter plots show 50% and 90% credible interval contours. The posteriors on n is peaked $n \approx 4/3$ and for values of f_0 close to the lower end of the detector's low frequency sensitivity. In this region of parameters space, the effect of nonlinear tides is degenerate with chirp mass, causing a secondary peak in the chirp mass posterior. It can be seen from the $\delta\phi$ - \mathcal{M} plot (lower left) that large phase shifts due to non-linear tides are due to points in parameter space where a value of chirp mass can be found that compensates for the phase shift of the nonlinear tides.

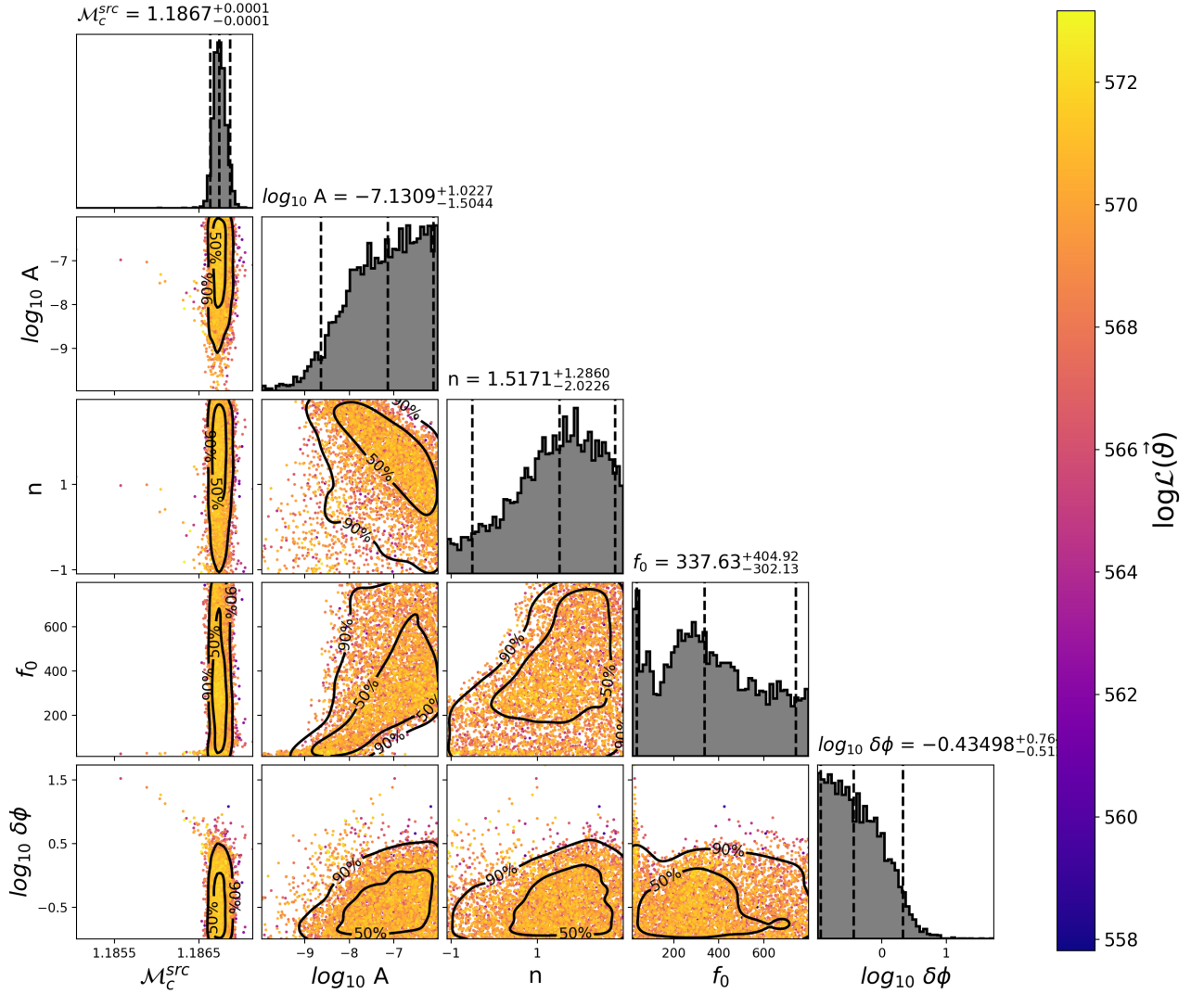


Figure 3. The marginalized posterior distributions for the uniform mass prior and a f_0 in the range 15 and 800 Hz. The vertical lines on the marginalized histograms display the 5th, 50th, and 95th percentiles of the posteriors. The three-detector network log likelihood ratio for each sample is given on the color-bar. The posterior scatter plots show 50% and 90% credible interval contours. One can still see several samples in the posteriors where the chirp mass degeneracy occurs, but for these priors there is a much larger region of parameter space where high matches can be found between the standard model and the nonlinear tide model. Notice in the f_0 - A posterior, the region with large values of A and small f_0 is excluded from the 90% credible interval.